

## In-situ synthesis of phthalocyanines on electrospun TiO<sub>2</sub> nanofiber by solvothermal process for photocatalytic degradation of methylene blue

Selin GÜMRÜKÇÜ<sup>1</sup>, Mukaddes ÖZÇEŞMECİ<sup>1</sup>, Esmâ SEZER<sup>1</sup>, Belkıs USTAMEHMETOĞLU<sup>1</sup>, Esin HAMURYUDAN\*<sup>1</sup>

Department of Chemistry, Faculty of Science and Letters, İstanbul Technical University, İstanbul, Turkey

Received: 07.08.2021 • Accepted/Published Online: 22.10.2021 • Final Version: 20.12.2021

**Abstract:** Titanium dioxide/phthalocyanine (TiO<sub>2</sub>/Pc), TiO<sub>2</sub>/fluor containing phthalocyanine (TiO<sub>2</sub>/FPC), and TiO<sub>2</sub>/fluor containing cobalt phthalocyanine (TiO<sub>2</sub>/FCoPc) had been successfully fabricated by a simple combination of phthalocyanines obtained by in-situ synthesis on the surface of TiO<sub>2</sub> nanofibers prepared by electrospinning. Scanning electron microscopy micrographs and X-ray diffraction analysis indicated that the phthalocyanines uniformly immobilized on the surface of TiO<sub>2</sub> nanofibers. Photocatalytic activity of TiO<sub>2</sub>/TiO<sub>2</sub>/Pc, TiO<sub>2</sub>/FPC, TiO<sub>2</sub>/FCoPc nanofibers for methylene blue in water was comparatively investigated firstly by ultraviolet-visible absorption measurements with time, and kinetic parameters were calculated. Results indicated that the obtained TiO<sub>2</sub>/Pc, TiO<sub>2</sub>/FPC and TiO<sub>2</sub>/FCoPc exhibited high photocatalytic activity for the degradation of methylene blue and TiO<sub>2</sub>/FCoPc was found the best. It showed similar or higher activities than related studies and can be suggested as a promising candidate for environmental and energy applications.

**Key words:** Phthalocyanine, nanofiber, electrospinning, photodegradation, photocatalytic

### 1. Introduction

Synthetic organic dyes are widely used in chemical, petrochemical, food processing or textile industries, many of which are discharged to the environment by wastewater, causing many ecological problems [1–3]. In recent years, the removal of these dyes from wastewater has become a major and urgent need for a clean and comfortable environment. Several methods including chemical oxidation [4], adsorption [5], electrochemical treatment [6], microbiological degradation [7], and photocatalytic degradation [8] have been developed to resolve these problems. Among these methods, photocatalysis is one of the most attractive methods in this field because of its low cost and the formation of non-toxic by-products [9,10].

Titanium dioxide (TiO<sub>2</sub>) is one of the most important semiconductor materials and photocatalyst because of its low cost, easy availability, high chemical stability, anti-corrosive properties, and non-toxicity [11, 12].

Phthalocyanines (Pcs) are also known as attractive alternatives for photocatalytic decomposition based on the visible light of organic dyes. They have two absorptions in the UV region of 300–400 nm (B band) and 600–700 nm region (Q band) resulting from  $\pi$ - $\pi^*$  transitions. In addition, besides this property, metallophthalocyanines possess excellent resistance to chemical degradation and good photosensitivity [13–17]. The synthetic flexibility of phthalocyanines offers great possibilities to change the desired properties. For example, fluoro-substituted metallophthalocyanines have been reported to be efficient catalysts for many applications [18–22]. Electron withdrawing fluorine substituents decrease the electron density of the macrocyclic ring and increase the redox potential, catalytic activity, and stability [18–28].

Pc nanostructures were successfully grown on the TiO<sub>2</sub> nanofibers substrates by in-situ one-pot synthesis with the advantage of saving time and simplicity.

Electrospinning is a way of obtaining nanofibers from various polymer solutions and melting them by applying electrical forces [29–31]. There are remarkable studies on the preparation of electrospun nanofibers to suit or enable various applications by changing the solution and processing parameters during production [32, 33]. Nanofibers are of considerable interest in a wide range of applications nowadays, including catalyst supports, drug delivery systems, sensors/biosensors, and photocatalysts, due to the multiple benefits they provide [34–36]. This approach makes it possible to produce nanofibers by combining many objects with a mixture of different polymers or by making modifications to the surfaces of the resulting fibers [37, 38].

\* Correspondence: esin@itu.edu.tr

Because of the above advantages, combining the photoresponsive property of both  $\text{TiO}_2$  and phthalocyanines to prepare a photocatalyst is important in the degradation of organic dyes. In this study, methylene blue (MB) was studied because MB is a common industrial organic dye and overdose of MB dye may cause harmful effects on human health, such as accelerated heart rhythm, vomiting, tissue necrosis [3, 39, 40]. In these considerations, here, we attempted to design photocatalysts that can be efficient in the photocatalytic degradation of methylene blue (MB) under ultraviolet (UV) irradiation. Also, it aims to evaluate the photocatalytic efficiency of both the central metal cation as cobalt and the fluorinated peripheral groups. For these purposes, in this study, pure  $\text{TiO}_2$ ,  $\text{TiO}_2$ /phthalocyanine ( $\text{TiO}_2$ /Pc),  $\text{TiO}_2$ /2,9(10),16(17),23(24)-tetrakis{[2',3',5',6'-tetrafluoro-4'-(octafluoropentoxy)benzyloxy]phthalocyanine ( $\text{TiO}_2$ /FPc) and  $\text{TiO}_2$ /2,9(10),16(17),23(24)-tetrakis{[2',3',5',6'-tetrafluoro-4'-(octafluoropentoxy) benzyloxy]phthalocyaninato} cobalt(II) ( $\text{TiO}_2$ /FCoPc) photocatalysts based on  $\text{TiO}_2$  nanofibers were prepared by combining the electrospinning and solvothermal techniques. These photocatalysts were characterized by using X-ray diffraction (XRD), scanning electron microscopy (SEM), energy dispersive X-ray (EDX), and UV-Visible absorption spectra. Their photocatalytic properties were investigated by UV-Visible absorption spectrophotometric measurements, and kinetic parameters were obtained. Recycling properties of the photocatalytic degradation of MB using  $\text{TiO}_2$ /FCoPc as the optimum photocatalyst was tested in order to gain information about multiple uses and stability of this material.

## 2. Experimental

### 2.1. Materials

Polyvinylpyrrolidone (PVP,  $M_w = 1.300.000$ ) powder, phthalonitrile, ethanol, acetic acid, titanium(IV) butoxide (TBT), ethylene glycol, methylene blue (MB) were obtained from Sigma Aldrich. They were all used without any purification. Distilled water was supplied from Merck Millipore Milli-Q ultrapure water system (Merck Millipore, Molsheim, France). Distilled water was used throughout all experiments. 4-[2',3',5',6'-tetrafluoro-4'-(octafluoropentoxy)benzyloxy]phthalonitrile was synthesized and purified as our previous report [25].

### 2.2. Preparation of photocatalysts

#### 2.2.1. Preparation of $\text{TiO}_2$ nanofibers

In a capped bottle, 2 g PVP powder was dissolved in acetic acid (5 mL) and absolute ethanol (9 mL) mixture under vigorous stirring for 2 h. Then, TBT (2 g) was added to this homogeneous solution followed by stirring for 2 more hours to make a precursor solution. In order to have  $\text{TiO}_2$  nanofibers, a flat, aluminum foil-covered plate was located at a fixed distance of 15 cm from the needle tip. 12 kV (Gamma High Voltage Research) voltage was supplied, and electrospinning was carried out at room temperature. The feeding rate of the PVP solution was controlled by a digitally controlled syringe pump (New Era, NE-300), which was adjusted to a volume flow ratio of 1 mL/h. With the applied voltage, the solvent was evaporated and charged polymers were deposited on the Al foil collector in the form of nanofibers.  $\text{TiO}_2$  nanofibers were made by the calcination of obtained nanofibers at 550 °C for 2 h (Figure 1).

#### 2.2.2. Fabrication of $\text{TiO}_2$ /Pc and $\text{TiO}_2$ /FPc nanofibers

A mixture of  $\text{TiO}_2$  nanofibers (15 mg), ammonium molybdate (1 mg), phthalonitrile derivatives (phthalonitrile (12.8 mg) for  $\text{TiO}_2$ /Pc or 4-[2',3',5',6'-tetrafluoro-4'-(octafluoropentoxy)benzyloxy]phthalonitrile (53.6 mg) for  $\text{TiO}_2$ /FPc and ethylene glycol (40 mL) were put into a teflon-lined stainless autoclave with the capacity of 50 mL. The autoclave was closed, and the reaction mixture was reacted at 160 °C for 20 h. The reaction system was closed, and the mixture was allowed to reach

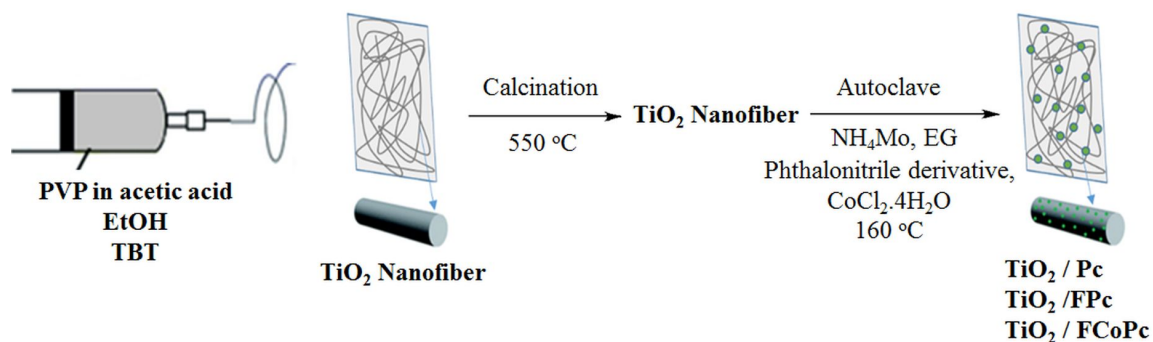


Figure 1. The schematic procedure of preparation of the  $\text{TiO}_2$ /Pc,  $\text{TiO}_2$ /FPc, and  $\text{TiO}_2$ /FCoPc nanofibers.

room temperature. The obtained samples were washed with distilled water under ultrasound (at three times) and ethyl alcohol to remove any ionic residue. Finally, the products were dried in vacuo (Figure 1).

### 2.2.3. Fabrication of TiO<sub>2</sub>/FCoPc nanofibers

The autoclave was charged with 4-[2',3',5',6'-tetrafluoro-4'-(octafluoropentoxy)benzyloxy]phthalonitrile (53.6 mg), CoCl<sub>2</sub>·4H<sub>2</sub>O (5 mg), ammonium molybdate (1 mg), TiO<sub>2</sub> nanofibers (15 mg) and ethylene glycol (40 mL). This mixture was stirred at 160 °C for 24 h, then the reaction system was cooled down to room temperature. The product was washed successively with distilled water and ethanol, then, dried at 50 °C for 10 h (Figure 1).

### 2.3. Characterization

Surface morphologies of the fabricated nanofibers were investigated using a scanning electron microscope (SEM; QUANTA 400 F) after sputter coating with ultra-thin gold film. Energy dispersive X-ray (EDX) spectroscopy was used to analyze the composition of samples. Crystal structure analysis was carried out using X-ray diffraction (XRD) (Rigaku D/Max-IIIC diffractometer) with Cu-K $\alpha$  line of 1.54 Å radiation and 2 $\theta$  range of 10–90°. UV-Visible absorption spectra were recorded on a Perkin Elmer Lambda 45 UV-Visible spectrophotometer.

### 2.4. Photocatalytic degradation test

The photodegradation studies of MB solution were examined under the UV lamp by using synthesized nanofibers.

Photocatalytic degradation of MB for different nanofibers was investigated

(i) in the dark with the presence of photocatalysts,

(ii) in the UV-light irradiation with the presence of the photocatalysts.

UV-A light (= 365 nm, UV-A 320 nm to 400 nm) was used in all the experiments [41]. Photocatalytic degradation of the MB was performed in a petri dish containing 100 mL dye solution with 10 mg of the photocatalyst sample. In order to figure out the photocatalysis activity of the samples, 5 ppm MB aqueous solution was prepared. The solution was stirred in dark for 30 min to realize adsorption-desorption equilibrium between the photocatalyst sample and the organic molecules. Changes in the concentrations of dyes were measured using UV-Vis spectrometer. The reaction was carried out at room temperature for 2 h. Samples of MB dye solution at different time intervals were analyzed during this time.

## 3. Results and discussion

In this work, pure TiO<sub>2</sub>, TiO<sub>2</sub>/Pc, TiO<sub>2</sub>/FPc, and TiO<sub>2</sub>/FCoPc nanofibers (Figure 2) were synthesized by combining the electrospinning and solvothermal techniques, and resulting nanofibers were characterized by SEM and XRD measurements. Detailed investigation of photocatalytic degradation of MB by using these nanofibers was also performed by kinetic measurements.

The morphological properties of these nanofibers were investigated by SEM (Figure 3). Figure 3a shows SEM images of the electrospun TiO<sub>2</sub> nanofibers before solvothermal treatment. SEM images of calcinated TiO<sub>2</sub> nanofibers at 550°C suggested smooth surface nanofibers with diameters in the range of 250–350 nm. The fabricated sample appeared as a non-woven nanofiber morphology after solvothermal treatment. A comparison between the SEM images of TiO<sub>2</sub>/Pc, TiO<sub>2</sub>/FPc and TiO<sub>2</sub>/FCoPc nanofibers in Figures 3b–3d, respectively with TiO<sub>2</sub> nanofibers clearly indicating that different types of Pc nanostructures were grown on the surface of TiO<sub>2</sub> nanofibers and gained beneficial properties such as large surface-to-volume ratio morphology. The morphology of FPc and FCoPc nanostructures grown on TiO<sub>2</sub> nanofibers changed from the nanowires to nanoflowers in Figures 3c and 3d, compatible with results from the literature [42].

It is clearly seen that different types of Pc nanostructures grow on the surface of TiO<sub>2</sub> nanofibers when different precursors are used according to the SEM images of TiO<sub>2</sub>/Pc, TiO<sub>2</sub>/FPc, and TiO<sub>2</sub>/FCoPc nanofibers in Figures 3b–3d. The average diameters of the TiO<sub>2</sub>, TiO<sub>2</sub>/Pc, TiO<sub>2</sub>/FPc, and TiO<sub>2</sub>/FCoPc nanofibers were calculated from the SEM images and found approximately as 0.45, 0.5, 0.7, and 0.8  $\mu$ m, respectively. It shows that Pc nanostructures did not grow on the surface of TiO<sub>2</sub> nanofibers when phthalonitrile compound was used as a precursor in the preparation of TiO<sub>2</sub>/Pc photocatalyst. It was clearly seen that when using 4-[2',3',5',6'-tetrafluoro-4'-(octafluoropentoxy)benzyloxy]phthalonitrile (for TiO<sub>2</sub>/FPc) FPc nanostructures grow on the surface of TiO<sub>2</sub> nanofibers. In addition, 4-[2',3',5',6'-tetrafluoro-4'-(octafluoropentoxy)benzyloxy]phthalonitrile used in the preparation of the TiO<sub>2</sub>/FCoPc photocatalyst were reacted with CoCl<sub>2</sub>·4H<sub>2</sub>O to synthesize FCoPc molecules in situ. FCoPc molecules were collected as nanoflowers on the surface of TiO<sub>2</sub> nanofibers. In the case of TiO<sub>2</sub>/FPc and TiO<sub>2</sub>/FCoPc nanofibers, 4-[2',3',5',6'-tetrafluoro-4'-(octafluoropentoxy)benzyloxy]phthalonitrile was homogeneously dispersed in TiO<sub>2</sub> nanofibers by the interaction of hydrogen bonds formed between the fluorinated groups of the phthalonitrile derivative and the surface hydroxyl groups of TiO<sub>2</sub> nanofibers. Since the presence of Co in addition to fluorinated groups also enhances the interaction, the TiO<sub>2</sub>/FCoPc nanofiber has the largest diameter, hence the largest surface area, and increased interaction with MB is expected.

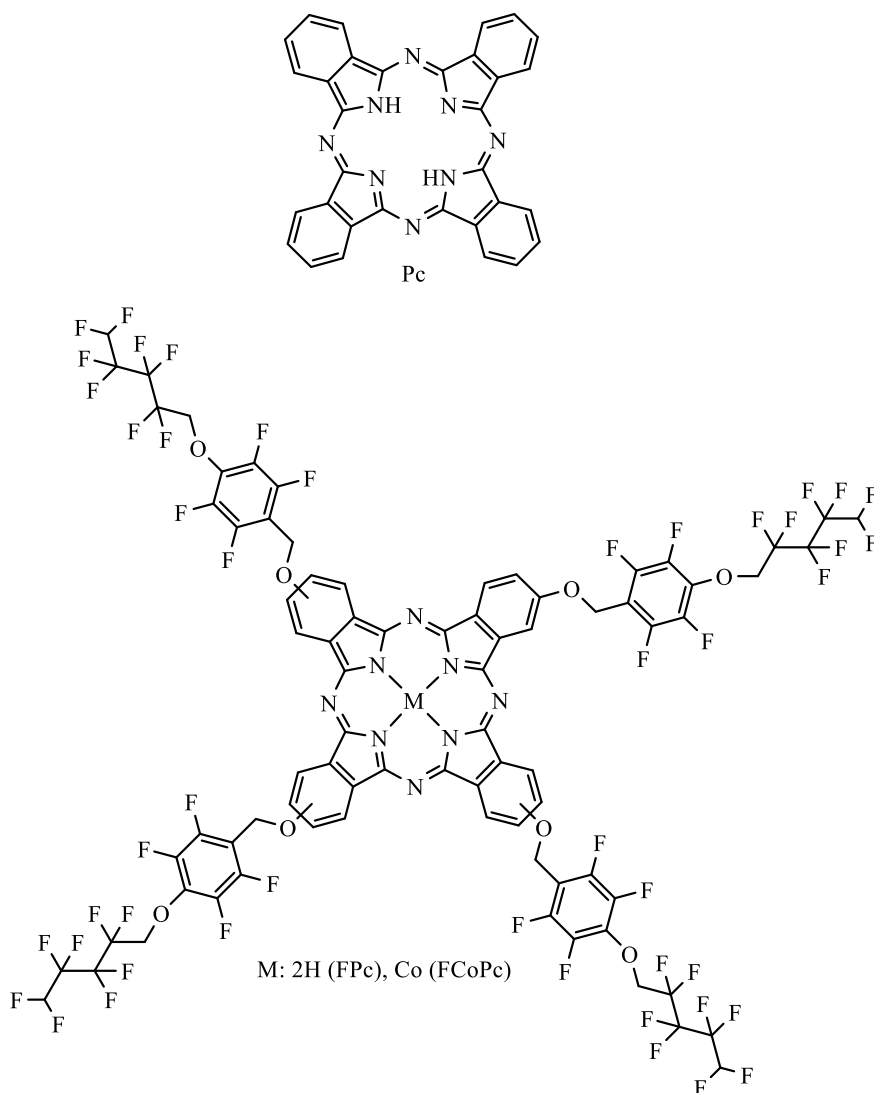


**Figure 2.** The structures of Pc, FPc, and FCoPc complexes.

According to EDX analysis results of  $\text{TiO}_2$ ,  $\text{TiO}_2/\text{Pc}$ ,  $\text{TiO}_2/\text{FPc}$ , and  $\text{TiO}_2/\text{FCoPc}$  nanofibers, the weight percentage (Wt %) of each element was shown in Table 1. Ti and O elements were reported to exist in pure  $\text{TiO}_2$  electrospun nanofibers; on the other hand, Ti, N, F, and Co occurred in  $\text{TiO}_2/\text{Pc}$ ,  $\text{TiO}_2/\text{FPc}$ , and  $\text{TiO}_2/\text{FCoPc}$  nanofibers, respectively.

The crystal structures of  $\text{TiO}_2$ ,  $\text{TiO}_2/\text{Pc}$ ,  $\text{TiO}_2/\text{FPc}$ , and  $\text{TiO}_2/\text{FCoPc}$  nanofiber photocatalyst were characterized via X-ray diffraction spectrometer (XRD) (Figure 4). It was observed that the developed pure  $\text{TiO}_2$  nanofiber was a combination of anatase and brookite rather than a fully anatase structure. Anatase peaks at  $25.3^\circ$  (101),  $37.9^\circ$  (004),  $47.7^\circ$  (200), and  $54.7^\circ$  (002) and a minor brookite phase at  $30.8^\circ$  (121) can be seen [43]. As suggested in the literature, the presence of broad peaks around  $14.8^\circ$  (200),  $21.1^\circ$  to  $30.4^\circ$  (100), and at  $42^\circ$  to  $46^\circ$  (100) [44, 45] for  $\text{TiO}_2/\text{FCoPc}$  and broad peaks around  $15.7^\circ$  to  $30.2^\circ$  (100) [46] for  $\text{TiO}_2/\text{FPc}$  support to the formation of different Pc's on  $\text{TiO}_2$  nanofiber.

The performances of pure  $\text{TiO}_2$ ,  $\text{TiO}_2/\text{Pc}$ ,  $\text{TiO}_2/\text{FPc}$ , and  $\text{TiO}_2/\text{FCoPc}$  nanofiber photocatalysts were also evaluated on the degradation of MB that is a typical dye pollutant in industrial wastewater. Photogenerated electrons cause the degradation of MB. Change in absorbance of MB at 664 nm with time was measured under dark and irradiation, and, from the initial ( $C_0$ ) and the concentration at any time ( $C$ ) of MB solution, the ratio of concentrations ( $C/C_0$ ) was determined (Figure 5). In order to establish the adsorption-desorption equilibrium of MB solution, MB solution was stirred in the dark for 30 min before the irradiation in all cases (Figure 5 inset).

Change of MB concentration with time suggested first-order reaction kinetics as reported in the literature [47] where MB concentration was related with the reaction time via the following equation 1;

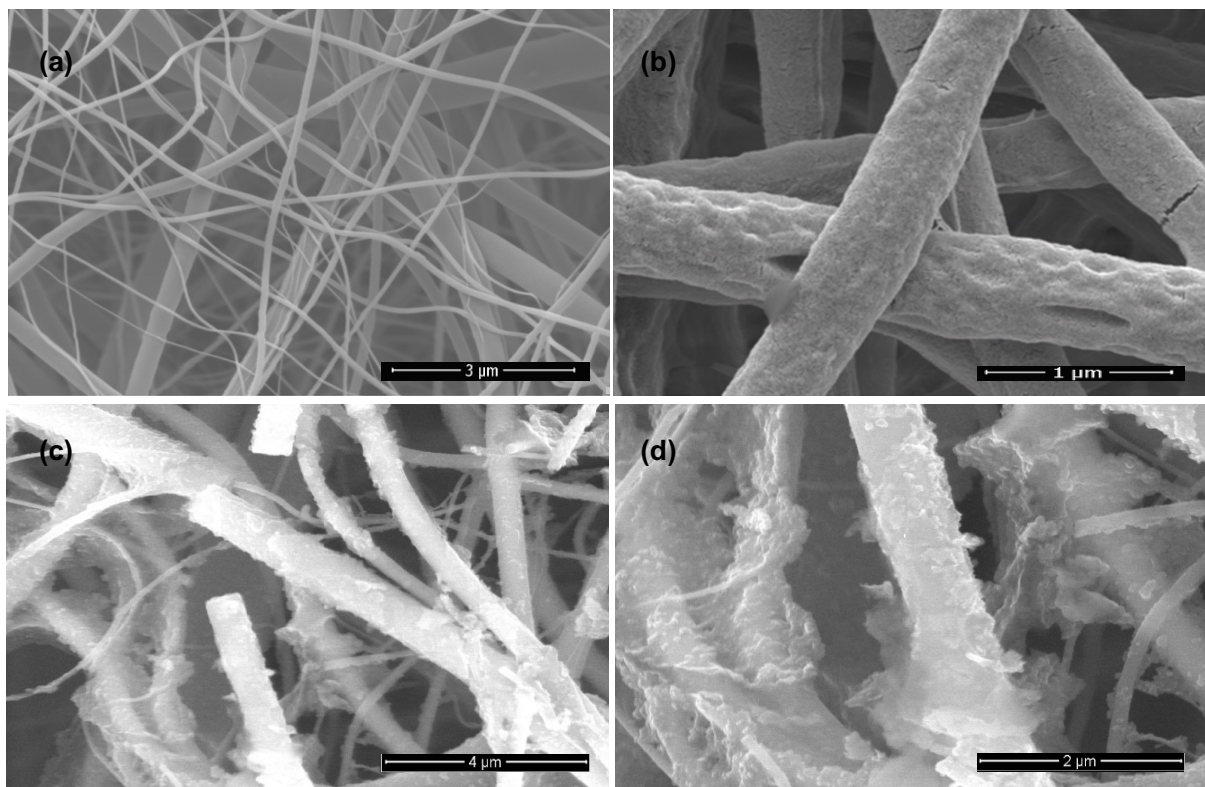


Figure 3. SEM images of (a)  $\text{TiO}_2$ , (b)  $\text{TiO}_2/\text{Pc}$ , (c)  $\text{TiO}_2/\text{FPc}$ , and (d)  $\text{TiO}_2/\text{FCoPc}$  nanofibers.

Table 1. EDX results of (a)  $\text{TiO}_2$ , (b)  $\text{TiO}_2/\text{Pc}$ , (c)  $\text{TiO}_2/\text{FPc}$  and (d)  $\text{TiO}_2/\text{FCoPc}$  nanofibers.

Element	Wt%			
	(a)	(b)	(c)	(d)
Ti			49.57	48.06
O	50.29	50.35	34.57	35.46
N	49.70	42.27	5.37	4.38
F		7.37	10.48	11.51
Co				0.58
Total	100.00	100.00	100.00	100.00

$$\ln \frac{C}{C_0} = -kt \quad (\text{Equation-1})$$

Here,  $k$  is a rate constant of the photodegradation of MB reaction,  $t$  is time, and  $C$  is the concentration of MB dye solution at a specific irradiation time.  $k$  values were obtained from the slope of the straight-lines of two regions (Region I = 0–60 minutes, Region II = 60–120 min) for the plot of  $\ln(C/C_0)$  versus time (Figure 6a, b).

According to the results given in Table 2, the  $k$  values in region I ( $k_I$ ) were almost 10 times lower than the  $k$  values in region II ( $k_{II}$ ), and  $\text{TiO}_2/\text{Pc}$  and  $\text{TiO}_2/\text{FCoPc}$  catalysts had the highest values in region I and region II, respectively. These results indicated that, although the interaction rate of  $\text{TiO}_2/\text{Pc}$  was faster than the others,  $\text{TiO}_2/\text{FPc}$  and  $\text{TiO}_2/\text{FCoPc}$  seem more effective as the reaction progress (Figure 6a, b).

The degradation rate ( $D\%$ ) was calculated with the following equation-2 (Figure 7):

$$D\% = \frac{C_0 - C}{C_0} \times 100\% \quad (\text{Equation-2})$$

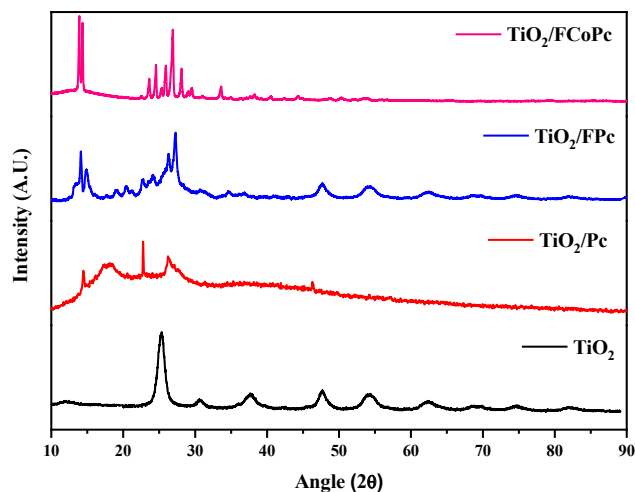


**Figure 4.** XRD patterns of  $\text{TiO}_2$ ,  $\text{TiO}_2/\text{Pc}$ ,  $\text{TiO}_2/\text{FPc}$  and  $\text{TiO}_2/\text{FCoPc}$  nanofibers.

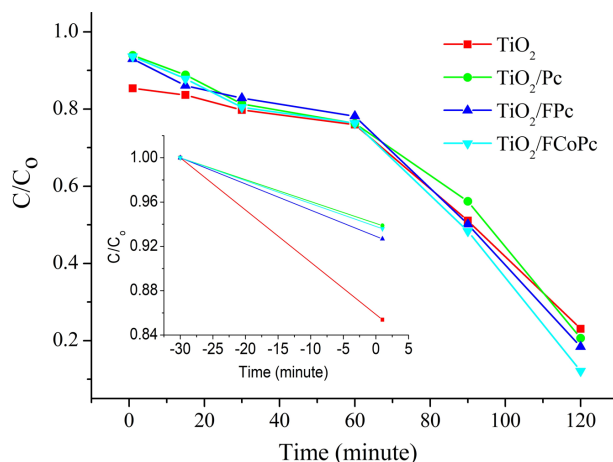


**Figure 5.**  $C/C_0$ -time graphs for the photocatalytic degradation of MB for  $\text{TiO}_2$ ,  $\text{TiO}_2/\text{Pc}$ ,  $\text{TiO}_2/\text{FPc}$  and  $\text{TiO}_2/\text{FCoPc}$  nanofibers.

The photocatalytic reactivity order was found as  $\text{TiO}_2/\text{FCoPc} > \text{TiO}_2/\text{FPc} > \text{TiO}_2/\text{Pc} > \text{TiO}_2$ . The corresponding degradation rates of MB reached about 88% within 120 min for  $\text{TiO}_2/\text{FCoPc}$ , which was in parallel with  $k$  values, due to the largest surface area of the  $\text{TiO}_2/\text{FCoPc}$  nanofibers as can be seen from SEM images (Figure 3d).

To determine the photocatalyst's stability, which is critical for their practical applications, the  $\text{TiO}_2/\text{FCoPc}$  was recovered by washing distilled water and used many times to degrade fresh MB solutions. Each time, the catalyst was dried in an oven at  $50^\circ\text{C}$ , without any further modification. Figure 8 shows that, after reuse, the  $\text{TiO}_2/\text{FCoPc}$  nanofiber retained high catalytic activity (100% to 98.5% and 95.51% by 1st, 2nd use, and 3rd use, respectively) with only approximately 6% loss in photocatalytic performance after the 3rd cycle.

According to these results, it can be suggested that the efficiency of  $\text{TiO}_2/\text{FCoPc}$  as a photocatalyst in photocatalytic degradation reactions is similar or higher than the related studies in the literature [48–50] and can be suggested as a promising candidate for the removal of organic pollutants from wastewater.

Based on the studies in the literature on photocatalytic degradation of organic pollutants in aqueous solutions [51–55], a possible mechanism for photocatalytic degradation of MB in UV light irradiation with  $\text{FCoPc}/\text{TiO}_2$  nanospun was schematically clarified in Figure 9, and the mechanism for photocatalytic degradation of MB was suggested as follows (Equations a-i):

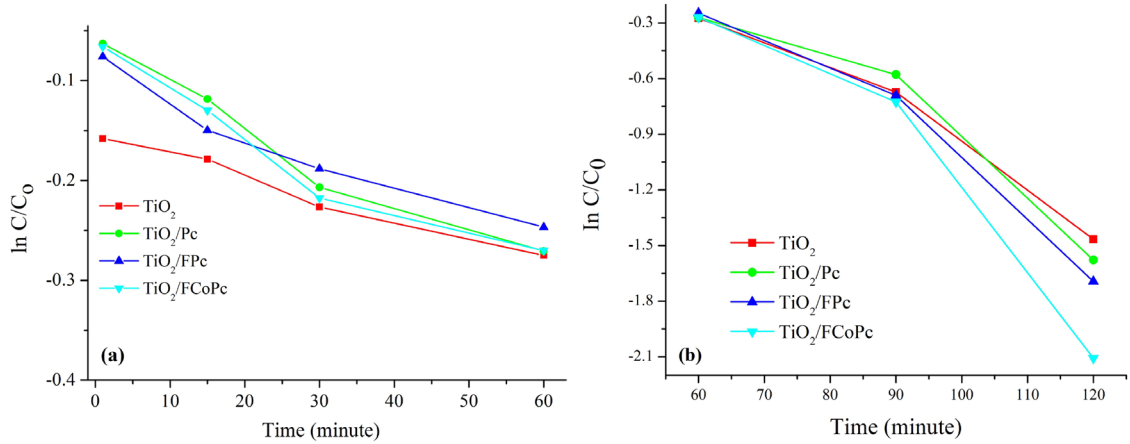


**Figure 6.** a)  $\ln C/C_0$ -time (region I), b)  $\ln C/C_0$ -time (region II) graphs for the photocatalytic degradation of MB for  $\text{TiO}_2$ ,  $\text{TiO}_2/\text{Pc}$ ,  $\text{TiO}_2/\text{FPc}$  and  $\text{TiO}_2/\text{FCoPc}$  nanofibers.

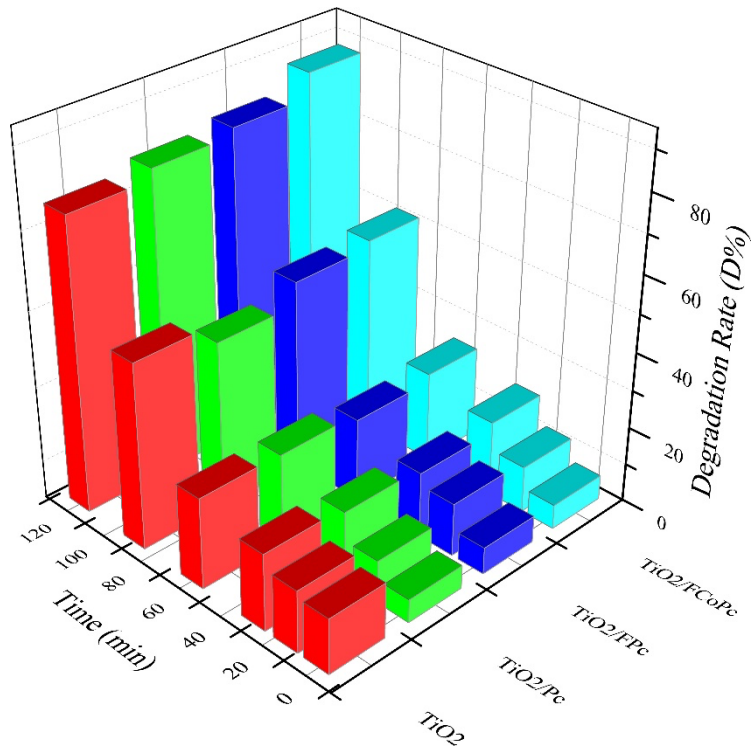
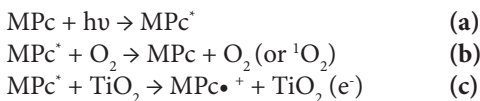


**Figure 7.** Photodegradation rate of MB for  $\text{TiO}_2$ ,  $\text{TiO}_2/\text{Pc}$ ,  $\text{TiO}_2/\text{FPc}$  and  $\text{TiO}_2/\text{FCoPc}$  nanofibers.



$\text{TiO}_2$  nanofibers were first photoexcited to generate electron/hole ( $e^-/h^+$ ) pairs. The electrons on the conduction band (CB) of  $\text{TiO}_2$  can be trapped to the  $\text{O}_2$  for generation of  $\cdot\text{O}_2^-$ , which is the most necessary active material for photocatalytic degradation of MB. Photogenerated holes on the valence band (VB) of  $\text{TiO}_2$  were expected to react with  $\text{H}_2\text{O}$  or  $\text{OH}^-$  to create  $\cdot\text{OH}$  because the potential of occurrence was lower than the VB of  $\text{TiO}_2$ .

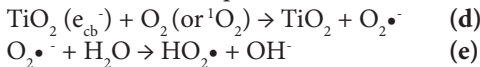


**Table 2.** Effect of different type of photocatalysts on the rate constant  $k$  and the total removal of photocatalytic MB degradation.

Sample name	$k$ ( $\text{min}^{-1}$ )		Total removal (%)
	Region I	Region II	
$\text{TiO}_2$	0.0020	0.0199	77
$\text{TiO}_2/\text{Pc}$	0.0036	0.0218	80
$\text{TiO}_2/\text{FPc}$	0.0028	0.0240	82
$\text{TiO}_2/\text{FCoPc}$	0.0031	0.0310	88

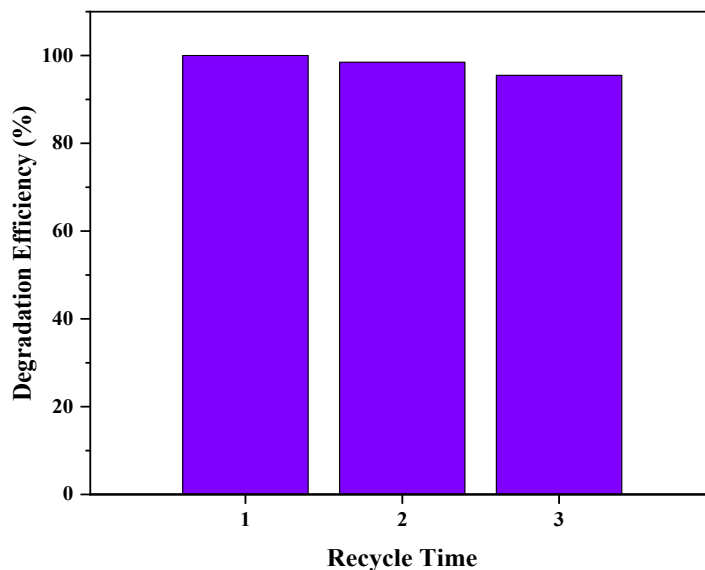


**Figure 8.** Recycling properties of the photocatalytic degradation of MB using  $\text{TiO}_2/\text{FCoPc}$  as photocatalyst.

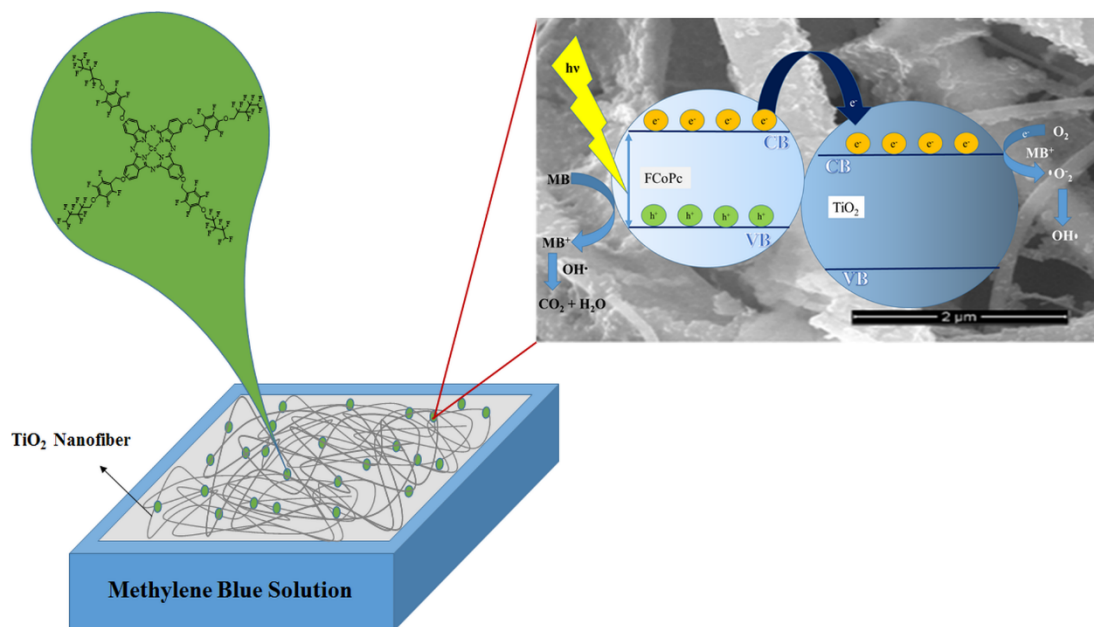
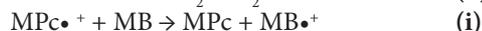
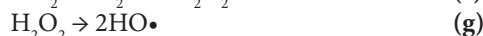
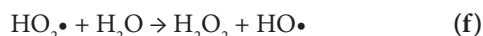


**Figure 9.** Schematic view of the degradation mechanism for MB by  $\text{TiO}_2/\text{FCoPc}$  photocatalyst.



The TiO<sub>2</sub> nanofibers serve as an electron trap for the activated surface adsorbed FCoPc dye. The trapped electron stimulates active oxygen species for later growth. Additionally, the active oxygen species, the by-produced radical cation FCoPc•<sup>+</sup> has already interacted with MB and induces MB photodegradation. Because no valence band hole is created in the TiO<sub>2</sub> nanofibrous, the nanofibrous FCoPc/TiO<sub>2</sub> avoids recombination of the internal charge. TiO<sub>2</sub> only acts as an electron mediator in this cycle, and the dye as a sensitizer.

#### 4. Conclusion

TiO<sub>2</sub> nanofiber was successfully fabricated from TBT precursor and firstly in-situ synthesis of Pc's on electrospun TiO<sub>2</sub> nanofiber was performed by the solvothermal process for photocatalytic degradation of MB. For this purpose, photocatalytic activity of a new type of fluor containing phthalocyanine (FPC) was comparatively investigated with non-fluorinated Pc and fluor containing cobalt Pc (FCoPc). Here, the effect of cobalt metal ion and peripheral fluorinated groups on the design of the photocatalyst was studied. The structures and morphologies of TiO<sub>2</sub>/Pc nanofibers were characterized using XRD, SEM, EDX, and UV-Vis absorption spectra.

The kinetic studies of photocatalytic degradation showed that while the catalytic effects of photodegradation of the Pcs in the dark are less than that of TiO<sub>2</sub>, Pcs have absorption in the UV region, which increases light efficiency, and showed better catalytic effect under light. The TiO<sub>2</sub>/FCoPc nanofibers exhibited a higher catalytic activity of photodegradation for MB than the pure TiO<sub>2</sub>, TiO<sub>2</sub>/Pc, or TiO<sub>2</sub>/FPC nanofibers under UV-light irradiation after 90 min due to the advantage of fluorinated groups. The presence of cobalt improves this efficiency. According to recycling results, TiO<sub>2</sub>/FCoPc nanofiber was found to be suitable for multiple uses. Based on all results, TiO<sub>2</sub>/FCoPc photocatalyst may be a promising candidate for the purification of organic pollutants from wastewater.

#### Acknowledgments

This work was supported by the Research Fund of the İstanbul Technical University.

#### References

1. Correia VM, Stephenson T, Judd S. Characterisation of textile wastewaters. *Environmental Technology* 1994; 15: 917-929. doi:10.1080/09593339409385500
2. Weber EJ, Adams RL. Chemical-and sediment-mediated reduction of the azo dye disperse blue 79. *Environmental Science & Technology* 1995; 29: 1163-1170.
3. Liu T, Hu T, Hu C, Lang JP. Synthesis, crystallographic characterization of a novel iron porphyrinate and its application as a photocatalyst for degradation of methylene blue under visible light irradiation. *Inorganic Chemistry Communication* 2018; 90: 26-28. doi: 10.1016/j.inoche.2018.01.027
4. Dutta K, Mukhopadhyay S, Bhattacharjee S, Chaudhuri B. Chemical oxidation of methylene blue using a Fenton-like reaction. *Journal of Hazardous Materials* 2001; 84: 57-71. doi: 10.1016/S0304-3894(01)00202-3
5. Körbahti BK, Artut K, Geçgel C, Özer A. Electrochemical decolorization of textile dyes and removal of metal ions from textile dye and metal ion binary mixtures. *Chemical Engineering Journal* 2011; 173: 677-688. doi: 10.1016/j.ccej.2011.02.018
6. Chatzisyneon E, Xekoukoulotakis NP, Coz A, Kalogerakis N, Mantzavinos D. Electrochemical treatment of textile dyes and dyehouse effluents. *Journal of Hazardous Materials* 2006; 137: 998-1007. doi: 10.1016/j.jhazmat.2006.03.032
7. Saratale R, Saratale G, Kalyani D, Chang JS, Govindwar S. Enhanced decolorization and biodegradation of textile azo dye Scarlet R by using developed microbial consortium-GR. *Bioresource Technology* 2009; 100: 2493-2500. doi: 10.1016/j.biortech.2008.12.013
8. Gupta VK, Pathania D, Agarwal S, Singh P. Adsorptional photocatalytic degradation of methylene blue onto pectin-CuS nanocomposite under solar light. *Journal of Hazardous Materials* 2012; 243: 179-186. doi: 10.1016/j.jhazmat.2012.10.018
9. Height MJ, Pratsinis SE, Mekasuwandumrong O, Praserttham P. Ag-ZnO catalysts for UV-photodegradation of methylene blue. *Applied Catalysis B: Environmental* 2006; 63: 305-312. doi: 10.1016/j.apcatb.2005.10.018
10. Jiang RB, Li BX, Fang CH, Wang JF. Metal/semiconductor hybrid nanostructures for plasmon-enhanced applications. *Advanced Materials* 2014; 26: 5274-5309. doi: 10.1002/adma.201400203

11. Linsebigler AL, Lu GQ, Yates JT. Photocatalysis on TiO<sub>2</sub> surfaces: principles, mechanisms, and selected results. *Chemical Reviews* 1995; 95: 735-738.
12. Hoffmann MR, Martin ST, Choi W, Bahnemann DW. Environmental applications of semiconductor photocatalysis. *Chemical Reviews* 1995; 95: 69-96.
13. Bayrak R, Albay C, Koç M, Altın İ, Değirmencioglu İ et al. Preparation of phthalocyanine/TiO<sub>2</sub> nanocomposites for photocatalytic removal of toxic Cr(VI) ions. *Process Safety and Environmental Protection* 2016; 102: 294-302. doi: 10.1016/j.psep.2016.03.023
14. Mahmiani Y, Sevim AM, Gül A. Photocatalytic degradation of 4-chlorophenol under visible light by using TiO<sub>2</sub> catalysts impregnated with Co(II) and Zn(II) phthalocyanine derivatives. *Journal of Photochemistry and Photobiology A: Chemistry* 2016; 321: 24-32. doi:10.1016/j.jphotochem.2015.12.015
15. Mahmiani Y., Sevim AM, Gül A. Photocatalytic degradation of persistent organic pollutants under visible irradiation by TiO<sub>2</sub> catalysts sensitized with Zn(II) and Co(II) tetracarboxy-phthalocyanines. *Journal of Porphyrins and Phthalocyanines* 2016; 20: 1190-1199. doi: 10.1142/S108842461650084X
16. Wieder ME, Hone DC, Cook MJ, Handsley MM, Gavriloic J et al. Intracellular photodynamic therapy with photosensitizer-nanoparticle conjugates: cancer therapy using a "Trojan horse". *Photochemical and Photobiological Sciences* 2006; 5: 727-734. doi: 10.1039/B602830F
17. Hone DC, Walker PI, Evans-Gowing R, FitzGerald S, Beeby A et al. Generation of cytotoxic singlet oxygen via phthalocyanine-stabilized gold nanoparticles: A potential delivery vehicle for photodynamic therapy. *Langmuir* 2002; 18: 2985-2987. doi: 10.1021/la0256230
18. Koca A, Özçeşmeci M, Hamuryudan E. Substituents effects to the electrochemical, and in situ spectroelectrochemical behavior of metallophthalocyanines: Electrocatalytic application for hydrogen evolution reaction. *Electroanalysis* 2010; 22 (14): 1623-1633. doi: 10.1002/elan.200900545
19. Carrión EN, Loas A, Patel HH, Pelmus M, Ramji K et al. Fluoroalkyl phthalocyanines: Bioinspired catalytic materials. *Journal of Porphyrins and Phthalocyanines* 2018; 22: 371-397. doi: 10.1142/S1088424618500189
20. Qiu T, Xu X, Qian X. Fluorous biphasic oxidation of ethyl benzene and benzyl alcohol catalyzed by perfluoroalkylphthalocyanine complexes. *Journal of Chemical Technology and Biotechnology*. 2009; 84: 1051-1055. doi: 10.1002/jctb.2132
21. Aktaş A, Pişkin M, Durmuş M, Biyıklıoğlu Z, Synthesis, photophysical and photochemical properties of zinc phthalocyanines bearing fluoro-functionalized substituents. *Journal of Luminescence* 2014; 145: 899-906. doi: 10.1016/j.jlumin.2013.09.019
22. Aktaş A, Acar İ, Saka ET, Biyıklıoğlu Z, Kantekin H. Fluoro functional groups substituted cobalt(II), iron(II) phthalocyanines and their catalytic properties on benzyl alcohol oxidation. *Journal of Inclusion Phenomena and Macrocyclic Chemistry* 2016; 86: 183-190. doi: 10.1007/s10847-016-0650-z
23. Özçeşmeci M, Nar I, Hamuryudan E. Synthesis and electrochemical and spectroelectrochemical characterization of chloromanganese (III) phthalocyanines. *Turkish Journal of Chemistry* 2014; 38: 1064-1072. doi: 10.3906/kim-1405-43
24. Schollhorn B, Germain JP, Pauly A, Maleysson C, Blanc JP. Influence of peripheral electron-withdrawing substituents on the conductivity of zinc phthalocyanine in the presence of gases. Part 1: reducing gases. *Thin Solid Films* 1998; 326: 245-250. doi: 10.1016/S0040-6090(98)00553-7
25. Özçeşmeci M, Özkan E, Hamuryudan E. Synthesis, characterization, and aggregation properties of functionalized polyfluorinated metallophthalocyanines. *Journal of Porphyrins and Phthalocyanines* 2013; 17: 972-979. doi: 10.1142/S1088424613500764
26. Handa M, Suzuki A, Shoji S, Kasuga K, Sogabe K. Spectral and electrochemical properties of vanadyl hexadecafluorophthalocyanine. *Inorganica Chimica Acta* 1995; 230: 41-44. doi: 10.1016/0020-1693(94)04188-2
27. Koca A, Özkaya A, Selçukoğlu M, Hamuryudan E. Electrochemical and spectroelectrochemical characterization of the phthalocyanines with pentafluorobenzoyloxy substituents. *Electrochimica Acta* 2007; 52: 2683-2690. doi: 10.1016/j.electacta.2006.09.025
28. Özçeşmeci M, Özçeşmeci I, Sorar I, Hamuryudan E. Thin films of fluorinated groups substituted metallophthalocyanines as an optical material. *Inorganic Chemistry Communication* 2017; 86: 209-212. doi: 10.1016/j.inoche.2017.10.026
29. Bhardwaj N, Kundu SC. Electrospinning: A fascinating fiber fabrication technique *Biotechnology Advances* 2010; 28: 325-347. doi: 10.1016/j.biotechadv.2010.01.004
30. Li X, Chen W, Qian Q, Huang H, Chen Y et al. Electrospinning-based strategies for battery materials. *Advanced Functional Materials* 2021; 11: 202000845. doi: 10.1002/aenm.202000845
31. Cui J, Lu T, Li F, Wang Y, Lei J et al. Flexible and transparent composite nanofiber membrane that was fabricated via a "green" electrospinning method for efficient particulate matter 2.5 capture. *Journal of Colloid and Interface Science* 2021; 582: 506-514. doi: 10.1016/j.jcis.2020.08.075
32. Ray SS, Chen SS, Li CW, Nguyen NC, Nguyen HT. A comprehensive review: electrospinning technique for fabrication and surface modification of membranes for water treatment application. *RSC Advances* 2016; 6: 85495-85514. doi: 10.1039/C6RA14952A

33. Ejaz F, Boor A, Lalia S, Hashaikeh R. A review on electrospinning for membrane fabrication: Challenges and applications. *Desalination* 2015; 356: 15-30. doi: doi.org/10.1016/j.desal.2014.09.033
34. Esenturk İ, Gümrükçü S, Sert ABÖ, Kök FN, Döşler S et al. Silk-fibroin-containing nanofibers for topical sertaconazole delivery: preparation, characterization, and antifungal activity. *International Journal of Polymeric Materials and Polymeric Biomaterials* 2021; 70(9): 605-622. doi: 10.1080/00914037.2020.1740992
35. Uçar N, Nesrin Demirsoy N, Önen A, Karacan İ, Kızıldağ N et al. The effect of reduction methods and stabilizer (PVP) on the properties of polyacrylonitrile (PAN) composite nanofibers in the presence of nanosilver. *Journal of Materials Science* 2015; 50: 1855-1864. doi: 10.1007/s10853-014-8748-4
36. Lu L, Yang B, Zhai Y, Liu J. Electrospinning core-sheath piezoelectric microfibers for self-powered stitchable sensor. *Nano Energy* 2020; 76: 104966. doi: 10.1016/j.nanoen.2020.104966
37. Gümrükçü S, Sopruncuk V, Saraç B, Yüce E, Eckert J et al. Electrospun polyacrylonitrile/2-(acryloyloxy)ethyl ferrocenecarboxylate polymer blend nanofibers. *Molecular Systems Design & Engineering* 2021; 6: 476-492. doi: 10.1039/d1me00008j
38. Han C, Zhang M, Cao WQ, Cao MS. Electrospinning and in-situ hierarchical thermal treatment to tailor C–NiCo<sub>2</sub>O<sub>4</sub> nanofibers for tunable microwave absorption. *Carbon* 2021; 171: 953-962. doi: 10.1016/j.carbon.2020.09.067
39. Vallejo W, Diaz-Urube C, Cantillo A. Methylene blue photocatalytic degradation under visible irradiation on TiO<sub>2</sub> thin films sensitized with Cu and Zn tetracarboxy-phthalocyanines. *Journal of Photochemistry and Photobiology A: Chemistry* 2015; 299: 80-86. doi:10.1016/j.jphotochem.2014.11.009
40. Rafatullah M, Sulaiman O, Hashim R, Ahmad A. Adsorption of methylene blue on low-cost adsorbents: A review. *Journal of Hazardous Materials* 2010; 177: 70-80. doi: 10.1016/j.jhazmat.2009.12.047
41. Zor S, Budak B. Investigation of the effect of PAN and PAN/ZnO photocatalysts on 100% degradation of Congo red under UV visible light irradiation and lightless environment. *Turkish Journal of Chemistry* 2020; 44: 486-501. doi:10.3906/kim-1907-30
42. Zhang M, Shao C, Guo Z, Zhang Z, Mu J et al. Hierarchical nanostructures of copper(II) phthalocyanine on electrospun TiO<sub>2</sub> Nanofibers: controllable solvothermal-fabrication and enhanced visible photocatalytic properties. *ACS Applied Materials & Interfaces* 2011; 3: 369-377. doi: 10.1021/am100989a
43. Berki P, Reti B, Terzi K, Bountas I, Horvath E et al. The effect of titania precursor on the morphology of prepared TiO<sub>2</sub>/MWCNT nanocomposite materials, *Physica Status Solidi (B): Basic Research* 2014; 251(12): 2384-2388. doi: 10.1002/pssb.201451161
44. Kuzumoto Y, Matsuyama H, Kitamura M. Structural and electrical properties of fluorinated copper phthalocyanine toward organic photovoltaics: Post-annealing effect under pressure. *Japanese Journal of Applied Physics* 2014; 53: 04ER16. doi: 10.7567/JJAP.53.04ER16
45. Soliman HS, El-Barry AMA, Khosifan NM, El Nahass MM. Structural and electrical properties of thermally evaporated cobalt phthalocyanine (CoPc) thin films. *The European Physical Journal Applied Physics* 2007; 37: 1-9. doi: 10.1051/epjap:2006135
46. Basova TV, Kiselev VG, Dubkov IS, Latteyer F, Gromilov SA et al. Optical spectroscopy and XRD study of molecular orientation, polymorphism, and phase transitions in fluorinated vanadyl phthalocyanine thin films. *Journal of Physical Chemistry C* 2013; 117: 7097-7106. doi: 10.1021/jp4016257
47. Vasiljevic ZZ, Dojcinovic MP, Vujanecvic JD, Jankovic-Castvan I, Ognjanovic M et al. Photocatalytic degradation of methylene blue under natural sunlight using iron titanate nanoparticles prepared by a modified sol-gel method. *Royal Society Open Science* 2020; 7: 200708. doi: 10.1098/rsos.200708
48. Liu G, Liu S, Lu Q, Sun H, Xiu Z. BiVO<sub>4</sub>/cobalt phthalocyanine (CoPc) nanofiber heterostructures: synthesis, characterization and application in photodegradation of methylene blue. *RSC Advances* 2014; 4: 53402-53406. doi: 10.1039/c4ra08759c
49. Wan Y, Liang Q, Cong T, Wang X, Tao Y et al. Novel catalyst of zinc tetraamino-phthalocyanine supported by multi-walled carbon nanotubes with enhanced visible-light photocatalytic activity. *RSC Advances* 2015; 5: 66286-66293. doi: 10.1039/c5ra10462a
50. Guo Z, Shao C, Mu J, Zhang M, Zhang Z et al. Controllable fabrication of cadmium phthalocyanine nanostructures immobilized on electrospun polyacrylonitrile nanofibers with high photocatalytic properties under visible light. *Catalysis Communications* 2011; 12: 880-885. doi: 10.1016/j.catcom.2011.02.004
51. Wu CH, Chern JM. Kinetics of photocatalytic decomposition of methylene blue. *Industrial & Engineering Chemistry Research* 2006; 45: 6450-6457. doi: 10.1021/ie0602759
52. Guo Z, Chen B, Mu J, Zhang M, Zhang P et al. Iron phthalocyanine/TiO<sub>2</sub> nanofiber heterostructures with enhanced visible photocatalytic activity assisted with H<sub>2</sub>O<sub>2</sub>. *Journal of Hazardous Materials* 2012; 219-220: 156-163. doi: 10.1016/j.jhazmat.2012.03.068
53. Cabir B, Yurderi M, Caner N, Agirtas MS, Zahmakiran M et al. Methylene blue photocatalytic degradation under visible light irradiation on copper phthalocyanine-sensitized TiO<sub>2</sub> nanopowders. *Materials Science and Engineering B* 2017; 224: 9-17. doi: 10.1016/j.mseb.2017.06.017

54. Zhang M, Shao C, Guo Z, Zhang Z, Mu J et al. Highly efficient decomposition of organic dye by aqueous-solid phase transfer and in situ photocatalysis using hierarchical copper phthalocyanine hollow spheres. *ACS Applied Materials & Interfaces* 2011; 3: 2573-2578. doi: 10.1021/am200412t
55. Li K, Pang Y, Lu Q. In situ growth of copper(II) phthalocyanine sensitized electrospun  $\text{CeO}_2/\text{Bi}_2\text{MoO}_6$  nanofibers: a highly efficient photoelectrocatalyst towards degradation of tetracycline. *Inorganic Chemistry Frontiers* 2019; 6: 3215-3224. doi: 10.1039/c9qi00950g